

PAPER

Pressure effect on the magnetoresistivity of topological semimetal RhSn

To cite this article: Shuxiang Xu *et al* 2020 *J. Phys.: Condens. Matter* **32** 355601

View the [article online](#) for updates and enhancements.



IOP | ebooks™

Bringing together innovative digital publishing with leading authors from the global scientific community.

Start exploring the collection—download the first chapter of every title for free.

Pressure effect on the magnetoresistivity of topological semimetal RhSn

Shuxiang Xu^{1,2} , Sheng Xu^{3,4}, Jianping Sun^{1,2}, Bosen Wang^{1,2,5}, Yoshiya Uwatoko⁶, Tianlong Xia^{3,4} and Jinguang Cheng^{1,2,5,7} 

¹ Beijing National Laboratory for Condensed Matter Physics and Institute of Physics, Chinese Academy of Sciences, Beijing 100190, People's Republic of China

² School of Physical Sciences, University of Chinese Academy of Sciences, Beijing 100190, People's Republic of China

³ Department of Physics, Renmin University of China, Beijing 100872, People's Republic of China

⁴ Beijing Key Laboratory of Opto-electronic Functional Materials & Micro-nano Devices, Renmin University of China, Beijing 100872, People's Republic of China

⁵ Songshan Lake Materials Laboratory, Dongguan, Guangdong 523808, People's Republic of China

⁶ Institute for Solid State Physics, University of Tokyo, Kashiwa, Chiba 277-8581, Japan

E-mail: jgcheng@iphy.ac.cn

Received 10 February 2020, revised 11 April 2020

Accepted for publication 23 April 2020

Published 29 May 2020



CrossMark

Abstract

RhSn is a topological semimetal with chiral fermions. At ambient pressure, it exhibits large positive magnetoresistance (MR) and field-induced resistivity upturn at low temperatures. Here we report on the electrical transport properties of RhSn single crystal under various pressures. We find that with increasing pressure the temperature-dependent resistivity $\rho(T)$ of RhSn varies minutely, whereas the value of MR at low temperatures decreases significantly. The $\rho(T)$ data was fitted with the Bloch–Grüneisen model and the Debye temperature was extracted. Analyses of the nonlinear Hall conductivity with two-band model indicate that the carrier concentrations do not change significantly with pressure, but the mobilities for both electron and hole carriers are reduced monotonically, which can account for the significant reduction of MR under high pressures.

Keywords: topological semimetal, magnetoresistance, nonlinear Hall conductivity, pressure effect, high motilities

(Some figures may appear in colour only in the online journal)

1. Introduction

Topological semimetals (TSMs) have attracted tremendous research interest in recent years due to their exotic physical properties and potential applications. According to the momentum space distribution and degeneracy of the band-crossing points, TSMs can be classified into Dirac semimetal, Weyl semimetal, and node-line semimetal, etc [1]. Experimental realizations include the Dirac semimetal Na₃Bi [2–4] and Cd₃As₂ [5–9], the Weyl semimetal TaAs [10–12] and WTe₂ [13–16], and the node-line semimetal ZrSiS [17–19] and PbTaSe₂ [20–22], respectively. Recently, some new type

fermions have been discovered in TSMs as exemplified by the threefold-degenerate fermion in MoP [23–25] and WC [26, 27]. In addition, angle-resolved photoemission spectroscopy (ARPES) measurements on the CoSi with a chiral lattice have evidenced the presence of unconventional chiral fermions near the Fermi level, which are named spin-1 and charge-2 fermions at the Brillouin zone (BZ) center Γ and the BZ corner R , respectively [28]. However, the band splitting of CoSi induced by the spin–orbit coupling (SOC) is too small to be observed in ARPES [28–30]. In this regard, the new material RhSn that shares similar crystal and band structures as CoSi but has a stronger SOC is a more promising candidate material to study the unconventional chiral fermions [31].

⁷ Author to whom any correspondence should be addressed.

Very recently, some of us grown high-quality RhSn single crystals and investigated in detail the electronic and transport properties at ambient pressure (AP) [32]. RhSn crystallizes in a simple cubic structure with the space group P213 (no. 198) and is characterized as a multi-band system with high carrier mobilities. At low temperatures, it exhibits large unsaturated longitudinal magnetoresistance (MR) with $B \parallel [001]$ and nonlinear Hall resistivity. Pronounced dHvA quantum oscillations were observed and ten fundamental frequencies were extracted from the fast Fourier-transform analysis. Aided by the first-principles calculations, four frequencies have been identified as originating from the topological nontrivial electronlike pockets at Γ and R points and the rest stems from the trivial holelike pockets. For the frequencies of electronlike pockets, the extracted Berry phases are in good accordance with the large Chern number $C = \pm 4$ in the first-principles calculations with SOC. The Wannier charge center calculations without SOC show that the spin-1 (charge-2) fermions at Γ (R) of RhSn carry chiral charges -2 ($+2$), which are opposite to those of CoSi. The chiral fermions between RhSn and CoSi are reversed because of their opposite structure chirality. These results have been confirmed recently by the ARPES measurements [33].

In this work, we have studied the effect of pressure on the electrical transport properties of RhSn single crystal. We find that the resistivity $\rho(T)$ of RhSn is robust against pressure with a tiny change up to 11.5 GPa. However, the low-temperature MR decreases monotonically with increasing pressure, which has been ascribed to the reduction of carrier mobility according to the two-band model fitting to the nonlinear Hall conductivity. Our results indicate that the lattice compression by pressure can fine tune the electronic band structure of RhSn with chiral fermions.

2. Experimental

The high-quality RhSn single crystal was grown out of the Bi flux as described in [32], in which the detailed characterizations on the structural and physical properties at ambient pressure have also been reported. The resistivity of RhSn single crystal under various hydrostatic pressures was measured with the standard four-probe method by using the palm cubic anvil cell (CAC) apparatus. Details about the experimental setup can be found elsewhere [34, 35]. Glycerol was employed as the pressure transmitting medium and the pressure values were determined at room temperature by observing the characteristic phase transitions of bismuth. For our measurements with CAC, we always change pressure at room temperature, tighten the pressure cell at the target pressure, and then load it into a liquid-helium cryostat to measure the temperature dependence of resistivity at a given pressure.

3. Results and discussion

Figure 1 shows the temperature dependence of resistivity $\rho(T)$ for the RhSn single crystal under various pressures from 2 to 11.5 GPa. The metallic behavior of RhSn is

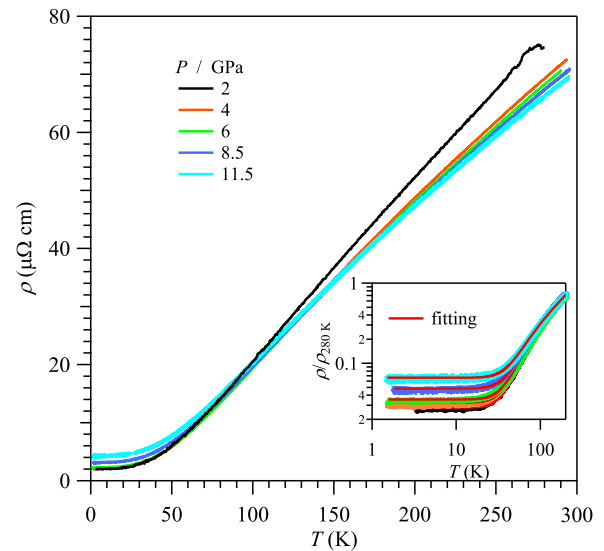


Figure 1. Temperature dependence of resistivity $\rho(T)$ for a RhSn single crystal under various pressures up to 11.5 GPa. Inset shows the normalized $\rho(T)$ curves in the double-logarithm scale. The solid red lines represent the fitting curves with the Bloch–Grüneisen formula (see text).

retained and no superconductivity was observed down to 1.5 K in the investigated pressure range. The absence of superconductivity might be related with the chiral lattice of RhSn, in which the lack of inversion symmetry would prevent the formation of conventional Cooper pairs with either spin-singlet or spin-triplet pairing [36]. When applying pressure from 2 to 4 GPa, the $\rho(T)$ at room temperature decreases from 78 to 70 $\mu\Omega$ cm, but the low-temperature resistivity is barely changed. Upon further increasing pressure to 6 GPa and above, the $\rho(T)$ at room temperature decreases by less than 1 $\mu\Omega$ cm per GPa, while the low-temperature resistivity is enhanced gradually, resulting in a reduction of residual resistivity ratio ($\text{RRR} = \rho(280 \text{ K})/\rho(2 \text{ K})$) under pressure. The residual resistivity $\rho(2 \text{ K}) \sim 3 \mu\Omega$ cm of RhSn at 2 GPa is about one order of magnitude smaller than that of CoSi $\sim 20 \mu\Omega$ cm [37]. The RRR is ~ 36 at 2 GPa and decreases to ~ 15 at 11.5 GPa, which is still larger than that of CoSi at similar pressure indicating the high quality of the studied RhSn single crystal.

As we know, the dominant scattering mechanism in the transport process of nonmagnetic metallic systems can be distinguished by fitting the $\rho(T)$ with the Bloch–Grüneisen formula [38, 39], viz

$$\rho(T) = \rho_0 + C \left(\frac{T}{\Theta_R} \right)^n \int_0^{\Theta_R/T} \frac{t^n}{(e^t - 1)(1 - e^{-t})} dt, \quad (1)$$

where ρ_0 is the residual resistivity, C is a material-specific constant, Θ_R is a characteristic temperature that is close to the Debye temperature Θ_D , and the exponent n can take the integer value of 2, 3 or 5, which corresponds to the dominant electron–electron, phonon–phonon, or electron–phonon scattering mechanism, respectively. As shown in the inset of figure 1, all $\rho(T)$ curves can be described excellently with $n = 5$ over

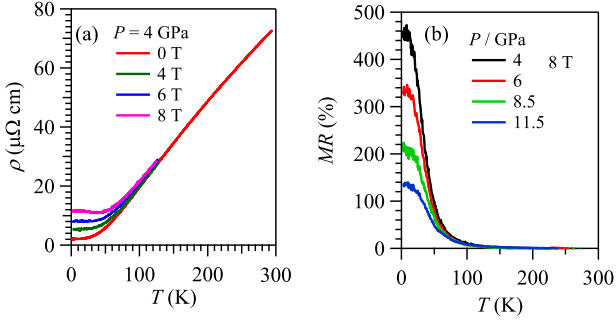


Figure 2. (a) Temperature dependence of resistivity $\rho(T)$ at 4 GPa for a RhSn single crystal under various magnetic fields up to 8 T. (b) Temperature dependence of magnetoresistance (MR) at 8 T under various pressures up to 11.5 GPa.

the whole temperature range (red solid lines), indicating that the electron–phonon scattering dominates the transport process under high pressures in RhSn. The obtained Θ_D from the fitting is 282 K at 2 GPa and keeps almost constant at about 270 ± 5 K in the investigated pressure range. The extracted Θ_D of RhSn under high pressures are also close to that of isostructural CoSi, i.e. ~ 300 K [37].

Figure 2(a) displays the $\rho(T)$ of RhSn at 4 GPa under various magnetic fields up to 8 T. The low-temperature $\rho(T)$ increases progressively with increasing magnetic field, and a weak upturn in $\rho(T)$ appears under 8 T. Similar positive MR behaviors are also observed for $\rho(T)$ at other pressures (no shown here). But the magnitude of MR is reduced gradually with increasing pressure. Figure 2(b) shows the temperature dependence of $\text{MR} \equiv [\rho(H)/\rho(0 \text{ T}) - 1] \times 100\%$ under 8 T at different pressures. As can be seen, $\text{MR}(T)$ increases rapidly upon cooling below 100 K; the $\text{MR}(2 \text{ K})$ reaches 450% at 4 GPa, but is reduced with increasing pressure to 135% at 11.5 GPa. A large, positive MR has been commonly observed in the TSMs such as Cd_3As_2 , TaAs, LaSb, WTe_2 , etc, and was ascribed to the electron–hole compensation and topological nontrivial band structures [8, 10, 18, 19, 26, 37, 40, 41]. But the magnitude of MR values of RhSn is much smaller than those of typical Dirac, Weyl and nodal-line semimetals [6, 19, 42], presumably due to the contributions from both topologically nontrivial electron and trivial hole carriers in RhSn.

Figure 3(a) displays the field-dependent MR at 2 K with $B||[111]$ under various pressures up to 11.5 GPa. The black dashed lines stand for the fitting results to a polynomial formula $\text{MR} \propto H^\alpha$, yielding an $\alpha = 3/2$ for the whole magnetic field range up to 8 T. Similar behavior is also observed at ambient pressure, and should be ascribed to the topological nontrivial electronlike bands at Γ and R in RhSn. In addition, the $\text{MR} \propto H^{3/2}$ behavior is retained in the whole pressure range, indicating that the topological characteristics of RhSn are extremely robust under high pressure. It should be noted that such an $H^{3/2}$ -dependent MR observed in RhSn is distinct from either the linear-in- H and non-saturated MR in the Dirac semimetals with the topological nontrivial bands or the H^2 -dependent MR with small magnitude in the normal metals with

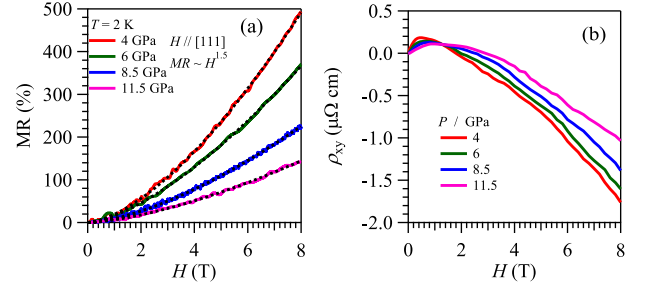


Figure 3. (a) Magnetic field dependence of MR at 2 K with $B||[111]$ for a RhSn single crystal under various pressures up to 11.5 GPa. The black dashed lines stand for the fitting results. (b) Magnetic field dependence of Hall resistivity ρ_{xy} at 2 K with $B||[111]$ for a RhSn single crystal under various pressures.

trivial band structures. Further studies are needed in order to achieve a better understanding of this behavior in RhSn.

Because we only measured the field dependence of MR at 2 K for each pressure, we cannot check the Kohler’s rule under pressure. Instead, we have replotted the MR data at AP in the form of MR versus (H/ρ_0) , and found that the Kohler’s rule is not well satisfied, especially for the temperatures above 30 K. Such a deviation from the Kohler’s rule is understandable since RhSn is a multi-band system with temperature-dependent carrier density and mobility [32]. We expect that the Kohler’s rule should also be violated under pressure given that the $H^{3/2}$ -dependence of MR and the band topology are retained in the investigated pressure range.

The Hall resistivity $\rho_{xy}(H)$ at 2 K for RhSn at various pressures are shown in figure 3(b). The overall behavior of $\rho_{xy}(H)$ under pressures resembles that at ambient pressure [32]. Especially, the deviation from the linear behavior of $\rho_{xy}(H)$ indicates that RhSn remains a multi-band system under pressure. In specific, the slope of $\rho_{xy}(H)$ or Hall coefficient changes sign with magnetic field, corresponding to the different roles of electron and hole carriers. The initial positive slope of $\rho_{xy}(H)$ indicates that there exist high-mobility hole pockets, while the negative slope at higher fields suggests the presence of electron pockets with higher concentration. When the pressure is increased, both the initial positive slope of $\rho_{xy}(H)$ and the negative slope at higher field are reduced gradually. This implies that the mobility of hole carrier is reduced and the concentration for electron pocket is enhanced by pressure.

In order to obtain the quantitative information about the carrier density and mobility as a function of pressure, we have fitted the Hall conductivity $\sigma_{xy} = \rho_{xy} / ((\rho_{xy})^2 + (\rho_{xx})^2)$ with the two-band model [32, 39], viz

$$\sigma_{xy} = \left(\frac{n_h \mu_h^2}{1 + (\mu_h B)^2} - \frac{n_e \mu_e^2}{1 + (\mu_e B)^2} \right) eB, \quad (2)$$

where $\mu_{e,h}$ and $n_{e,h}$ are the mobility and density of electron- and hole-type carriers, respectively. Similar two-band model analysis has also been applied at ambient pressure, and the $\mu_{e,h}$ and $n_{e,h}$ were extracted [32]. The value of magnetic field along $[111]$ is recalculated by multiplying $\cos(30^\circ)$ because the sample surface is not perpendicular to magnetic field perfectly. As

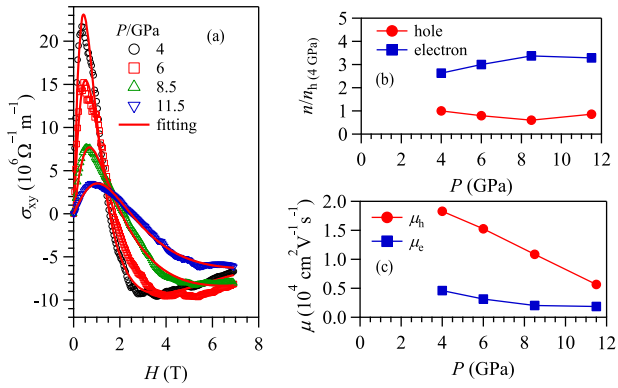


Figure 4. (a) Field dependence of the Hall conductivity under various pressures. (b) and (c) The pressure dependence of the normalized carrier densities and mobility of electron and hole extracted from figure 4(a) by two-band model fitting.

shown by the solid lines in figure 4(a), the $\sigma_{xy}(H)$ curves are well fitted and the obtained $n_{e,h}(P)$ and $\mu_{e,h}(P)$ at 2 K as a function of pressure are shown in figures 4(b) and (c), respectively. The carrier concentration of electron pocket is twice larger than that of hole, while the mobility of electron ($\sim 0.5 \times 10^4 \text{ cm}^2 \text{ V}^{-1} \text{ s}^{-1}$) is much less than that of hole ($\sim 1.9 \times 10^4 \text{ cm}^2 \text{ V}^{-1} \text{ s}^{-1}$) at 4 GPa, in line with the above qualitative arguments. As shown in figure 4(b), the concentration of electron-type carriers increases initially with pressure and reaches maximum at 8.5 GPa, while that of hole-type carriers exhibits opposite trends. In contrast, the mobilities of both electron- and hole-carriers are reduced over the whole pressure range; in particular, the mobility of holes decreases much faster than that of electrons with pressure. Overall, the carrier densities of both hole and electron are changed only slightly with pressure whereas the hole-carrier mobility decreases significantly with pressure.

As shown above, RhSn is a multi-band system with both electronlike and holelike Fermi surfaces (FSs). Although the current interest in RhSn is focused on the topologically non-trivial chiral fermions located at Γ and R points of the first Brillouin zone, there are several other topologically trivial holelike pockets near the Fermi energy, which has been well established by the dHvA oscillations and the first-principles calculations [32]. Since both topologically nontrivial electron and trivial hole carriers contribute to the electrical conduction, the temperature dependence of resistivity of RhSn looks like a normal metal. Nonetheless, the Hall resistivity is more sensitive to the carriers' characteristics, i.e. the hole carriers with higher mobility contribute to an initial positive slope at low fields, while the electron carriers with higher density produce a negative slope at high fields. Since the electrical transport properties of metals are usually dominated by the high-mobility carriers, the significant reduction of hole mobility should be responsible for the observed suppression of MR and RRR under pressure. This argument is further substantiated by the comparison of the hole-carrier mobility μ_h , MR and RRR as a function of pressure in figure 5. As can be seen, they all decrease monotonically with increasing pressure, signaling an intimate correlation among them. As we know, the

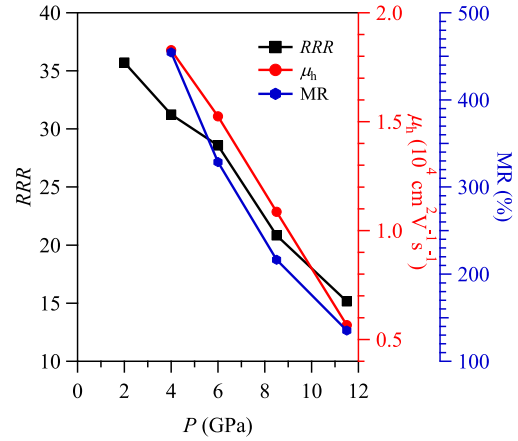


Figure 5. Pressure dependences of the residual resistivity ratio (RRR), the hole mobility μ_h , and MR at 8 T and 2 K.

carrier mobility is described by the relaxation time divided by the transport mass within semiclassical theory. Since the hole density only varies slightly with pressure, figure 4(b), the relaxation time of hole carriers associated with carrier scattering should not change significantly. Alternatively, the effective transport mass of hole might increase substantially, presumably due to the modification of band structures. Further theoretical studies on the band structures of RhSn under compression are needed to clarify this issue. On the other hand, the improvement of electron carrier density near the Fermi level under pressure indicates that the electrons are transferred from the other hole bands according to the Luttinger sum rule [43]. The enhancement of electron density of states would promote the electron scattering, resulting in a reduction of electron relaxation time and thus mobility with pressure as observed in figure 4(c). This will also lead to suppression of the MR.

4. Conclusion

In summary, we have studied the pressure effect on the electrical transport properties of RhSn single crystal with a cubic anvil cell apparatus up to 11.5 GPa. At ambient pressure, RhSn exhibits large positive MR and field-induced resistivity upturn at low temperatures. We found that the application of high pressure can barely change the resistivity $\rho(T)$ but the MR decreases monotonically with pressure. We have fitted the non-linear Hall conductivity and extracted the carrier density and mobility in terms of the two-band model. Our results indicate that the reduction of carrier mobility, especially that of the hole carriers, should be responsible for the suppression of low-temperature MR and the reduction of RRR. In addition, our work demonstrates that the electronic band structure of RhSn can be finely tuned through the lattice compression.

Acknowledgment

This work is supported by the National Key R & D Program of China (2018YFA0305700, 2019YFA0308602), the National Natural Science Foundation of China (11921004, 11904391,

11874422, 111834016, and 11874400), Beijing Natural Science Foundation (Z190008), the Strategic Priority Research Program and Key Research Program of Frontier Sciences of the Chinese Academy of Sciences (XDB25000000 and QYZDB-SSW-SLH013), and the CAS Interdisciplinary Innovation Team. T-LX also acknowledges support from the Fundamental Research Funds for the Central Universities, and the Research Funds of Renmin University of China (No. 19XNLG18, No. 18XNLG14).

ORCID iDs

Shuxiang Xu  <https://orcid.org/0000-0003-0727-6125>

Jinguang Cheng  <https://orcid.org/0000-0002-4969-1960>

References

- [1] Weng H, Dai X and Fang Z 2016 Topological semimetals predicted from first-principles calculations *J. Phys.: Condens. Matter* **28** 303001
- [2] Wang Z J, Sun Y, Chen X Q, Franchini C, Xu G, Weng H M, Dai X and Fang Z 2012 Dirac semimetal and topological phase transitions in A_3Bi ($A = Na, K, Rb$) *Phys. Rev. B* **85** 195302
- [3] Xiong J, Kushwaha S K, Liang T, Krizan J W, Hirschberger M, Wang W D, Cava R J and Ong N P 2015 Evidence for the chiral anomaly in the Dirac semimetal Na_3Bi *Science* **350** 413–6
- [4] Xu S Y *et al* 2015 Observation of Fermi arc surface states in a topological metal *Science* **347** 294–8
- [5] Wang Z J, Weng H M, Wu Q S, Dai X and Fang Z 2013 Three-dimensional Dirac semimetal and quantum transport in Cd_3As_2 *Phys. Rev. B* **88** 125427
- [6] He L P, Hong X C, Dong J K, Pan J, Zhang Z, Zhang J and Li S Y 2014 Quantum transport evidence for the three-dimensional Dirac semimetal phase in Cd_3As_2 *Phys. Rev. Lett.* **113** 246402
- [7] Neupane M *et al* 2014 Observation of a three-dimensional topological Dirac semimetal phase in high-mobility Cd_3As_2 *Nat. Commun.* **5** 3786
- [8] Liang T, Gibson Q, Ali M N, Liu M H, Cava R J and Ong N P 2015 Ultrahigh mobility and giant magnetoresistance in the Dirac semimetal Cd_3As_2 *Nat. Mater.* **14** 280–4
- [9] Zhao Y F *et al* 2015 Anisotropic Fermi surface and quantum limit transport in high mobility three-dimensional Dirac semimetal Cd_3As_2 *Phys. Rev. X* **5** 031037
- [10] Huang X C *et al* 2015 Observation of the chiral-anomaly-induced negative magnetoresistance in 3D Weyl semimetal TaAs *Phys. Rev. X* **5** 031023
- [11] Lv B Q *et al* 2015 Observation of Weyl nodes in TaAs *Nat. Phys.* **11** 724
- [12] Weng H M, Fang C, Fang Z, Bernevig B A and Dai X 2015 Weyl semimetal phase in noncentrosymmetric transition-metal monophosphides *Phys. Rev. X* **5** 011029
- [13] Bruno F Y *et al* 2016 Observation of large topologically trivial Fermi arcs in the candidate type-II Weyl semimetal WTe_2 *Phys. Rev. B* **94** 121112
- [14] Feng B J *et al* 2016 Spin texture in type-II Weyl semimetal WTe_2 *Phys. Rev. B* **94** 195134
- [15] Wang C L *et al* 2016 Observation of Fermi arc and its connection with bulk states in the candidate type-II Weyl semimetal WTe_2 *Phys. Rev. B* **94** 241119
- [16] Wu Y, Mou D X, Jo N H, Sun K W, Huang L N, Bud'ko S L, Canfield P C and Kaminski A 2016 Observation of Fermi arcs in the type-II Weyl semimetal candidate WTe_2 *Phys. Rev. B* **94** 121113
- [17] Xu Q N, Song Z D, Nie S M, Weng H M, Fang Z and Dai X 2015 Two-dimensional oxide topological insulator with iron-pnictide superconductor $LiFeAs$ structure *Phys. Rev. B* **92** 205310
- [18] Lv Y-Y, Zhang B-B, Li X, Yao S-H, Chen Y B, Zhou J, Zhang S-T, Lu M-H and Chen Y-F 2016 Extremely large and significantly anisotropic magnetoresistance in $ZrSiS$ single crystals *Appl. Phys. Lett.* **108** 244101
- [19] Singha R, Pariari A K, Satpati B and Mandal P 2017 Large nonsaturating magnetoresistance and signature of nondegenerate Dirac nodes in $ZrSiS$ *Proc. Natl Acad. Sci. USA* **114** 2468–73
- [20] Bian G *et al* 2016 Topological nodal-line fermions in spin-orbit metal $PbTaSe_2$ *Nat. Commun.* **7** 10556
- [21] Chang T R *et al* 2016 Topological Dirac surface states and superconducting pairing correlations in $PbTaSe_2$ *Phys. Rev. B* **93** 245130
- [22] Guan S Y, Chen P J, Chu M W, Sankar R, Chou F C, Jeng H T, Chang C S and Chuang T M 2016 Superconducting topological surface states in the noncentrosymmetric bulk superconductor $PbTaSe_2$ *Sci. Adv.* **2** 1600894
- [23] Zhu Z M, Winkler G W, Wu Q S, Li J and Soluyanov A A 2016 Triple point topological metals *Phys. Rev. X* **6** 031003
- [24] Lv B Q *et al* 2017 Observation of three-component fermions in the topological semimetal molybdenum phosphide *Nature* **546** 627
- [25] Kumar N *et al* 2019 Extremely high conductivity observed in the triple point topological metal MoP *Nat. Commun.* **10** 2475
- [26] He J B, Chen D, Zhu W L, Zhang S, Zhao L X, Ren Z A and Chen G F 2017 Magnetotransport properties of the triply degenerate node topological semimetal tungsten carbide *Phys. Rev. B* **95** 195165
- [27] Ma J Z *et al* 2018 Three-component fermions with surface Fermi arcs in tungsten carbide *Nat. Phys.* **14** 349
- [28] Rao Z *et al* 2019 Observation of unconventional chiral fermions with long Fermi arcs in $CoSi$ *Nature* **567** 496–9
- [29] Sanchez D S *et al* 2019 Topological chiral crystals with helicoid-arc quantum states *Nature* **567** 500–5
- [30] Takane D *et al* 2019 Observation of chiral fermions with a large topological charge and associated Fermi-arc surface states in $CoSi$ *Phys. Rev. Lett.* **122** 076402
- [31] Tang P, Zhou Q and Zhang S C 2017 Multiple types of topological fermions in transition metal silicides *Phys. Rev. Lett.* **119** 206402
- [32] Xu S, Zhou L Q, Wang H, Wang X Y, Su Y, Cheng P, Weng H M and Xia T L 2019 Quantum oscillations and electronic structure in the large-Chern number semimetal $RhSn$ *Phys. Rev. B* **100** 245146
- [33] Li H *et al* 2019 Chiral fermion reversal in chiral crystals *Nat. Commun.* **10** 5505
- [34] Cheng J G, Matsubayashi K, Nagasaki S, Hisada A, Hirayama T, Hedo M, Kagi H and Uwatoko Y 2014 Integrated-fin gasket for palm cubic-anvil high pressure apparatus *Rev. Sci. Instrum.* **85** 093097
- [35] Cheng J G, Wang B S, Sun J P and Uwatoko Y 2018 Cubic anvil cell apparatus for high-pressure and low-temperature physical property measurements *Chin. Phys. B* **27** 077403
- [36] Kaur R P, Agterberg D F and Sigrist M 2005 Helical vortex phase in the noncentrosymmetric $CePt_3Si$ *Phys. Rev. Lett.* **94** 137002
- [37] Wu D S, Mi Z Y, Li Y J, Wu W, Li P L, Song Y T, Liu G T, Li G and Luo J L 2019 Single crystal growth and magnetoresistivity of topological semimetal $CoSi$ *Chin. Phys. Lett.* **36** 077102
- [38] Cvijovic D 2011 The Bloch–Grüneisen function of arbitrary order and its series representations *Theor. Math. Phys.* **166** 37

- [39] Ziman J M 1960 *Electrons and Phonons* (Oxford: Clarendon)
- [40] Pletikosić I, Ali M N, Fedorov A V, Cava R J and Valla T 2014 Electronic structure basis for the extraordinary magnetoresistance in WTe_2 *Phys. Rev. Lett.* **113** 216601
- [41] Zeng L K *et al* 2016 Compensated semimetal LaSb with unsaturated magnetoresistance *Phys. Rev. Lett.* **117** 127204
- [42] Zhang C L, Yuan Z J, Jiang Q D, Tong B B, Zhang C, Xie X C and Jia S 2017 Electron scattering in tantalum monoarsenide *Phys. Rev. B* **95** 085202
- [43] Yamada R *et al* 2019 Large variation of Dirac semimetal state in perovskite CaIrO_3 with pressure-tuning of electron correlation *Phys. Rev. Lett.* **123** 216601